ELEKTROTEHNIŠKI VESTNIK 86(4): 169-180, 2022
ORIGINAL SCIENTIFIC PAPER

A novel sensorless fully synergetic control of the brushless doubly-fed induction machine integrated in a wind-energy conversion system with a fuzzy-based HCS MPPT algorithm and an extended Kalman filter

Mohammed Beghdadi, Katia Kouzi

Laboratory of semi-conductors and Functional Materials University Amar Telidji Laghouat, Algeria
E-mail : m.beghdadi@lagh-univ.dz

Abstract. The paper presents a novel fully sensorless synergetic control (power, torque and speed) of the brushless doubly-fed induction machine (BDFIM) integrated in a wind-energy conversion system (WECS) driven by a sensorless fuzzy-based hills climb search HCS MPPT algorithm comparable to the conventional tip speed ratio TSR MPPT algorithm. In the first stage, the proposed control algorithm involves a robust BDFIM control based on synergetic control theory. In the second stage, avoidance of the use of wind-speed sensors by employing an anemometer and maximization of the wind-energy extraction using fuzzy HCS MPPT, and in the last stage, the control scheme robustness is improved and an extended Kalman filter EKF is employed to estimate the rotor speed at high values of noise. According to the simulation results, the proposed wind-speed sensorless control algorithm proves the validity and effectiveness at parameter states.

Keywords: brushless doubly fed induction machine BDFIM, synergetic control SC, extended Kalman filter EKF, wind-energy conversion system WECS, fuzzy-based HCS MPPT algorithm, TSR MPPT algorithm.

Novo brezsenzorsko krmiljenje brezkrtačnega indukcijskega motorja z dvojnim napajanjem, integriranim v sistem za pretvorbo vetrne energije

V članku je predstavljeno novo brezsenzorsko sinergijsko krmiljenje (moči, navora in hitrosti) brezkrtačnega indukcijskega motorja z dvojnim napajanjem BDFIM, integriranim v sistem za pretvorbo vetrne energije WECS. Predlagani krmilni algoritem vključuje robustno krmiljenje BDFIM, ki temelji na sinergijski teoriji krmiljenja in mehki HCS MPPT za povečanje izkoristka vetrne energije. Z namenom povečanja robustnosti predlaganega krmiljenja smo uporabili razširjeni Kalmanov filter EKF za oceno hitrosti rotorja z upoštevanjem šuma. Eksperimentalni simulacijski rezultati potrjujejo predlagano krmiljenje pri različnih pogojih uporabe.

1 INTRODUCTION

The conventional energy (fossil) is becoming less and less available with an inevitable depletion. This energy has several drawbacks, the most important one is pollution. To solve the issue the world goes towards the exploiting of renewable clean energies like the solar and wind-energy, especially after the energy crisis in 1973 [1].

The wind energy is one of the most interesting renewable energies thanks to its wide availability and notable technical advancement in the generator construction and power electronic converters making it easier to be exploited while achieving high efficiency, optimal quality, and whatsoever pollution. Following the above, the installation of wind turbines worldwide has been growing fast in the last two decades to be over 440 GW and will reach 760 GW in the horizon of 2020 [2].

In the wind-energy conversion system (WECS), different types of generators can be used, like the permanent-magnet synchronous machines (PMSM), squirrel cage induction machines (SCIM) and the doubly-fed induction machine (DFIM). The last machine is interesting competitor of PMSM because of its low cost thanks to its construction simplicity, adjustable power factor, the fractional rated converter power (30% of the machine rated power) connected to the machine, its most important capability is separable control of active and reactive by its the direct power control (DPC. For this control to operate, the machine rotor must be fed by using brushes and slip rings which decreases the reliability of the system because of the need of replacing of the brushes and need to be known the rotor fragility.

The brushless doubly-fed induction machine (BDFIM or BDFIG) is an optimal solution to the DFIM drawbacks. It increases the robustness and reliability of the system thanks to the absence of the carbon brushes and slip rings making the machine work with an ease and the maintenance less frequently than for DFIM.

However, the variable-speed WECS with BDFIM needs both large operating speed range and a fast torque, to prevent disturbances and uncertainties (turbine torque

Received 13 October 2021
Accepted 23 March 2022

and parameter variations and lack of modeled dynamics). More advanced control methods are needed to meet the demands.

Recently, synergetic control takes a respectable place in the robust control community as well by industrial partners thanks to its successful implementation in power electronics and some industrial applications like battery charging [3], [4].

The main features of the synergetic control are, it is supporting parametric and nonparametric uncertainties, unlike is case with several other control techniques. Moreover, it provides a fast response, asymptotic stability of the closed-loop system in any operating state, and the system robustness in presence of parameter variations. Following the above, the paper presents novel synergetic control model of WECS with BDFIM.

For the system to extract the maximum possible power from a variable-speed wind, the system is driven by a maximum-power point-tracking MPPT algorithm which can be a sensor (with an anemometer) such as TSR MPPT, or a sensorless algorithm needing no anemometer. To use such methods as the power signal feedback PSR and the optimal torque control OTC the turbine characteristics need to be known, others such as the HCS do not need it. Though algorithms are most fast, the wind speed needs to be measured. As this cannot be done accurately, the wind speed values are approximative (wind speed is measured only in one point though it varies along the length of the blade, its correct value would be the average along blade radius) [6].

Moreover, to control and monitor WECS with BDFIM, the generator rotor position and speed needed to be known. It can be measured by a conventional mechanical sensor. Recently, there has been a growing industrial interest in high-performance sensorless WECSs for their many advantages, such as low cost, low maintenance, and high reliability. The paper presents an upgraded robust extended Kalman filter suppressing a large amount of the noise.

2 WECS Structure and its Mathematical Model

2.1 Brushless Doubly Fed Induction Machine Structure

BDFIM can be operated in both operational modes (motor and generator) needing two AC supplies with no direct electrical power feeding the machine rotor, the brush-slip ring system used in the conventional DFIM is thus no longer needed [7].

BDFIM is considered a radical solution for the brush-slip ring problem of the conventional DFIM though necessitating of some structural modifications to be affected in certain steps.

To solve the problem, operating with a cascade of two DFIM machines is needed. The two rotors are electrically interconnected to each other (direct or inverse connection) and mechanically coupled (see Fig. 1) [8], [9]. The rotor current is the same and the two stators are related to each other by the cross-magnetic coupling principle. this conception is known as a cascaded brushless doubly-fed induction machine (CBDFIM).

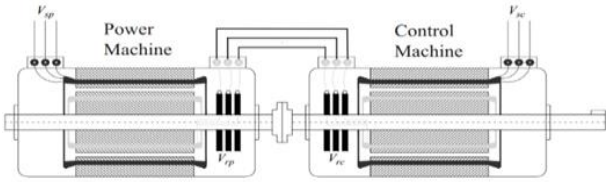

Figure 1. CBDFIM structure.

Researchers are taking an effort to have the two machines in one frame by integrating the two stators and common rotor to get a single-frame brushless doubly-fed induction machine SFBDFIM (see Fig. 2) [10].

Figure 2. SFBDFIM structure.

However, to reduce the congestion and make the system more practical, the two stator windings are placed in the same slot. This makes the machine smaller and similar to the conventional machine, i.e., a single brushless doubly-fed induction machine SBDFIM or simply BDFIM.

The focus of the paper is on BDFIM with one rotor of different structures such as wound, cage or nested rotor, and two stator windings. The power winding (PW) is directly connected to the grid and the other, the control winding (CW) is connected by a bidirectional converter [11] (see Fig. 3).

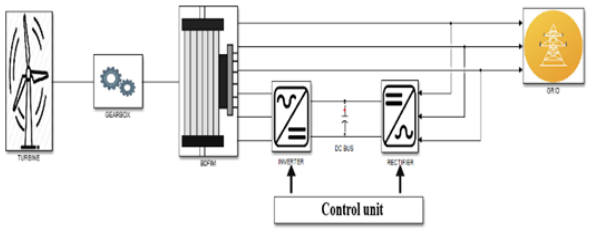

Figure 3. Wind-energy conversion system with BDFIM as a generator.

2.2 Mathematical model of the brushless doubly fed induction machine (BDFIM)

BDFIM works according to the principle of cross-magnetic coupling between PW and CW where one winding current can modify the other winding current by the machine rotor current when below two basics conditions are met [12], [13]:

$$\begin{cases} \omega_p = \omega_c + (P_1 + P_2).\Omega \\ N_r = P_1 + P_2 \end{cases} \quad (1)$$

These ω_p, ω_c, are the electrical pulses of PW and CW;
Ω is the rotor mechanic speed;
P_1 and P_2, are the pole numbers of PW and CW, respectively and N_r is the rotor nest number.

There are many ways to build the BDFIM mathematical model. The most commonly used one is based on dq transformer model when it is better to use a single frame for the entire system. As the power winding is fed by an invariable supply frequency it is absolutely an optimal choice. The system equations are [14]:

$$\begin{cases} V_{dp} = R_p I_{dp} + \dfrac{d\Psi_{dp}}{dt} - \omega_p \Psi_{qp} \\ V_{qp} = R_p I_{qp} + \dfrac{d\Psi_{qp}}{dt} + \omega_p \Psi_{dp} \\ 0 = R_r I_{dr} + \dfrac{d\Psi_{dr}}{dt} - (\omega_p - P_{pw}.\Omega)\Psi_{qr} \\ 0 = R_r I_{qr} + \dfrac{d\Psi_{qr}}{dt} + (\omega_p - P_{pw}\Omega)\Psi_{dr} \\ V_{dc} = R_c I_{dc} + \dfrac{d\Psi_{dc}}{dt} - (\omega_p - (P_{pw} + P_{cw}).\Omega)\Psi_{qc} \\ V_{qc} = R_c I_{qc} + \dfrac{d\Psi_{qc}}{dt} + (\omega_p - (P_{pw} + P_{cw}).\Omega)\Psi_{dc} \end{cases} \quad (2)$$

The magnetic equations are:

$$\begin{cases} \Psi_{dp} = L_p I_{dp} + M_p I_{dr} \\ \Psi_{qp} = L_p I_{qp} + M_p I_{qr} \\ \Psi_{dr} = L_r I_{dr} + M_p I_{dp} + M_c I_{dc} \\ \Psi_{qr} = L_r I_{qr} + M_p I_{qp} + M_c I_{qc} \\ \Psi_{dc} = L_c I_{dc} + M_c I_{dr} \\ \Psi_{qc} = L_c I_{qc} + M_c I_{qr} \end{cases} \quad (3)$$

The mechanic equations are:

$$\begin{cases} \dfrac{d\Omega}{dt} = \dfrac{T_{em} - T_r - f\Omega}{J} \\ T_e = P_1 M_p (I_{qp} I_{dr} - I_{dp} I_{qr}) + P_2 M_c (I_{qc} I_{dr} - I_{dc} I_{qr}) \end{cases} \quad (4)$$

Finally, the PW active and reactive power are:

$$\begin{cases} P_p = V_{qp} I_{qp} + V_{dp} I_{dp} \\ Q_p = V_{qp} I_{dp} - V_{dp} I_{qp} \end{cases} \quad (5)$$

where:

$V_{dp}, V_{qp}, V_{dc}, V_{qc}$ are dq-axes of PW and CW voltages;

$I_{dp}, I_{qp}, I_{dc}, I_{qc}, I_{dr}, I_{qr}$ are dq-axes of PW, CW and rotor currents;

R_p, R_c, R_r are the PW, CW and rotor resistors;

L_p, L_c, L_r are the PW, CW and rotor self-inductances;

M_p, M_c are the PW and CW mutual s;

$\Psi_{dp}, \Psi_{qp}, \Psi_{dc}, \Psi_{qc}, \Psi_{dr}, \Psi_{qr}$ are the dq-axes of PW, CW and rotor fluxes;

P_p, Q_p are the PW active and reactive power;

T_e is the machine electromagnetic torque;

T_r is the load torque;

F is the amping coefficient;

J is the inertia.

2.3 Modelling the Wind Turbine

The turbine blades are moved by the wind kinetic energy. They transform it to the mechanical power that rotates the turbine and the generator. To build the turbine mathematical model, the wind power needs to be defined:

$$P_w = \frac{1}{2}\rho S v^3 \quad (6)$$

where S, ρ, v are the circle area of the rotation's blades, the air density and the wind speed, respectively.

While the wind moves across the wind tower, it loses some speed due to the collisions with the turbine blades. Behind the tower, the wind always keeps moving so the turbine cannot take all the available wind kinetic energy. The limited extraction power is expressed as the power coefficient C_p, where $C_{p\text{-}max}$ is 16/27 is known as the Betz limit.

Many researches have tried to define an approximative formula for the power coefficient. In our paper, the below expression is used:

$$\begin{cases} C_p = 0.5176\left(\frac{116}{\lambda_i} - 0.4\beta - 5\right)e^{\frac{21}{\lambda_i}} \\ \frac{1}{\lambda_i} = \frac{1}{\lambda + 0.08\beta} - \frac{0.035}{\beta^3 + 1} \\ \lambda = \frac{R\omega_m}{v} \\ \omega_m = \Omega / G \end{cases} \quad (7)$$

These R is the blade radius;

β is the pitch angle of the blades;

ω_m is the turbine slow shift speed

and G is the gain of the gearbox.

So, the turbine mechanical power and torque with respect to the Betz limit are:

$$\begin{cases} P_T = \frac{1}{2} C_p \rho S v^3 \\ T_m = \frac{C_p \rho S v^3}{2\omega_m} \end{cases} \quad (8)$$

3 SYNERGETIC CONTROL

Synergy means working together. It is a team work where many factors collaborate to get a macro-effect bigger and better than getting it with every factor work alone. For example, many muscles intervene to assure one precise particular movement in the humane body knowing as muscle synergy (compound movement). It is very difficult to achieve where every muscle works independently from the others (isolation movement).

Any n-order nonlinear system is defined:

$$\dot{x} = f(x, u, t) \quad (9)$$

where x, u and t are the state vector, the control vector and the time respectively.

The synergetic control (SC) is gathering analytical approaches [15], [16] and its algorithm is set up in following steps:

Step 1: Choosing macro-variables Ψ_s with a simple linear relation or a combination with system variables [17] which reduces the order of the controlled system. So, one macro-variable is controlled for one control channel instead of many variables.

The major SC goal is to make the system follow the manifold Ψ_s=0.

Step 2: The dynamic evolution equation for the macro-variable is:

$$T\dot{\Psi}_s + \varphi(\Psi_s) = 0 \quad (10)$$

T is a control parameter and φ is a function of macro-variable, Ψ_s must be chosen carefully to assure the control stability to meeting the two conditions: φ(0) =0 and $\varphi(\Psi_s).\Psi_s > 0$.

It is easier to use $\varphi = \Psi_s$ to meet the above conditions. Its dynamic evolution equation is:

$$T\dot{\Psi}_s + \Psi_s = 0 \quad (11)$$

Step 3: Equation (11) is rewritten as:

$$T\frac{d\Psi_s}{dx}f(x,u,t) + \Psi_s = 0 \quad (12)$$

Step 4: Equation (13) provides control vector u:

$$u = g(x, \Psi_s, t, T) \quad (13)$$

The vector assures that the controlled system variables follow their references and that the performance is optimal.

3.1 The Proposed BDFIM Synergetic Control

The main DFIM and BDFIM advantage, is their capability of decoupling the active (torque and speed) and the reactive-power control. So, to control P_p, torque T_e or the speed is done by I_{qp}, while Q_p is controlled by I_{dp} and the previous currents are controlled by I_{qc} and I_{dc} respectively, which are controlled by the CW voltage [18].

The control algorithm is:

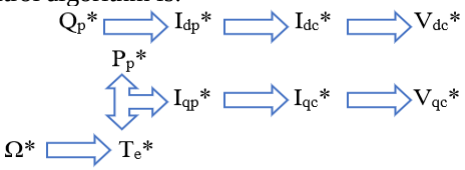

* Means the reference value of each parameter.

There are two control channels. The first is reserved for Q_p, and the second for P_p, T_e or the speed. Anyone can choose from the below shown, when integrating machine in WECS with any MPPT algorithm.

It is very useful to work with an oriented PW flux with a d-axe. This means $\Psi_{dp} = \Psi_p$ and $\Psi_{qp} = 0$. It simplifies the control and assures better performances. Using SC even with no oriented flux, the control still provides the required performance well as advantages of the proposed technique.

Below we show the development of the control process beginning with CW and PW current, active and reactive power, torque and the machine speed control.

As for any synergetic control, the first thing to do is choosing the macro-variable which takes the below form:

$$\Psi_{sc} = K_1(I_c^* - I_c) + K_2\int(I_c^* - I_c)dt \quad (14)$$

Where K_1 and K_2 are control parameters needing to be tuned to make the control faster and more stable.

Substituting the macro-variable in the dynamic equation we get:

$$T_1\left(K_1\left(\frac{dI_c^*}{dt} - \frac{dI_c}{dt}\right) + K_2(I_c^* - I_c) + K_1(I_c^* - I_c)\right) + K_2\int(I_c^* - I_c)dt = 0 \quad (15)$$

The PW flux equations shows that the rotor current can be written as a function of the PW flux and current. Substituting the rotor current and simplifying CW voltage equation we get:

$$\frac{dI_c}{dt} = \frac{1}{L_c}\left[V_c - R_cI_c - G_c\left(I_c, I_p, \Psi_p, \Omega, \omega_p, t\right)\right] \quad (16)$$

Whese G_c is the disturbing term of the I_c control defined as

$$G_c = \frac{M_c}{M_p}\frac{d\Psi_p}{dt} - \frac{M_cL_p}{M_p}\frac{dI_p}{dt} + j\left[\left(\omega_p - \left(P_{pw} + P_{cw}\right).\Omega\right)\left(L_cI_c + \frac{M_c}{M_p}\Psi_p - \frac{M_cL_p}{M_p}I_p\right)\right] \quad (17)$$

Solving the dynamic equation, the proper values of V_c are obtained to feed CW all having the desired I_c.

To get SCT-I_p, the same procedure applies.

Macro-variable Ψ_{sp} is:

$$\Psi_{sp} = K_3\left(I_p^* - I_p\right) + K_4\int\left(I_p^* - I_p\right)dt \quad (18)$$

and:

$$\frac{dI_p}{dt} = \frac{M_p}{L_pL_r\sigma_p}\left[M_c\frac{dI_c}{dt} - \frac{R_rL_p}{M_p} + G_p\left(I_c, I_p, \Psi_p, \Omega, \omega_p, t\right)\right] \quad (19)$$

where:

$$\begin{cases}\sigma_p = 1 - \frac{M_p{}^2}{L_pL_r} \\ G_p = \frac{L_r}{M_p}\frac{d\Psi_p}{dt} - \frac{R_r}{M_p}I_p + j\left[\left(\omega_p - P_{pw}\Omega\right)\left(L_cI_c + \frac{L_r}{M_p}\Psi_p - \frac{L_rL_p\sigma_p}{M_p}I_p\right)\right]\end{cases} \quad (20)$$

Solving (20), I_c* is obtained for the SCT-I_c controller.

To get the I_p reference I_p* from the P_p and Q_p references and assuming that BDFIM is connected to a strong grid by a controlled voltage (V_{dp}=0) and simplifying (5) we get:

$$\begin{cases}I_{dp}{}^* = \frac{Q_p{}^*}{V_{qp}} \\ I_{qp}{}^* = \frac{P_p{}^*}{V_{qp}}\end{cases} \quad (21)$$

Calculating I_c as a function of the I_p and neglecting the dynamic term of the current, the T_e formula is rewritten as a function of only the PW currents and flux:

$$T_e = (P_1 + P_2)\frac{w_p}{V_{qp}}I_{qp} + P_2\frac{2R_rL_p}{M_p{}^2(w_p - P_1\Omega)}|\Psi_p|I_{dp} - P_2\frac{R_r}{M_p{}^2(w_p - P_1\Omega)}\left(L_p{}^2|I_p|^2 - |\Psi_p|^2\right) \quad (22)$$

I_{qp}* can be obtained as:

$$I_{qp}{}^* = \frac{T_e{}^*V_{qp}}{(P_1+P_2)w_p} + G_{iqp}\left(|I_p|, I_{dp}, |\Psi_p|, \Omega, \omega_p, t\right) \quad (23)$$

where

$$G_{iqp} = \frac{V_{qp}}{(P_1+P_2)w_p}\left[-P_2\frac{2R_rL_p}{M_p{}^2(w_p - P_1\Omega)}|\Psi_p|I_{dp} + P_2\frac{R_r}{M_p{}^2(w_p - P_1\Omega)}\left(L_p{}^2|I_p|^2 - |\Psi_p|^2\right)\right] \quad (24)$$

The disturbing term (G_{iqp}) in the I_{qp}* equation is very small and can be neglected or taken in consideration by the feedback action [14].

By controlling the machine torque, it is very easy to control the speed. all we need is a synergetic controller to provide the torque reference from the reference speed.

the macro-variable is set as:

$$\Psi_{ss} = K_5(\Omega^* - \Omega) + K_6\int(\Omega^* - \Omega)dt \quad (25)$$

And the dynamic equation:

$$T_3(-K_5\dot{\Omega} + K_6(\Omega^* - \Omega) + K_5(\Omega^* - \Omega)) + K_6\int(\Omega^* - \Omega)dt = 0 \quad (26)$$

By substituting first equation (4) in (26) we obtain:

$$T_3(K_5\frac{T_{em}{}^* - T_r - f\Omega}{J} + K_6(\Omega^* - \Omega) + K_5(\Omega^* - \Omega)) + K_6\int(\Omega^* - \Omega)dt = 0 \quad (27)$$

Finally, from (27) we get:

$$T_{em}{}^* = \frac{-J}{T_3K_5}\left(T_3\left(K_6(\Omega^* - \Omega) + K_5(\Omega^* - \Omega)\right) + K_6\int(\Omega^* - \Omega)dt\right) - T_r - f\Omega \quad (28)$$

Using the torque reference, the rest of the control algorithm is continued.

3.2 Stability of the Proposed Synergetic Control

The SC stability is proven by the Lyapounov principle. The control is stable if product $V\dot{V} < 0$ where V is a positive function.

With $V = \Psi_s$, $\dot{V} = \dot{\Psi}_s$ and the eq (12): $\dot{V} = \dot{\Psi}_s = \frac{-\Psi_s}{T}$.

$$V\dot{V} = \Psi_s\dot{\Psi}_s = \frac{-\Psi_s}{T}\Psi_s = \frac{-{\Psi_s}^2}{T} < 0 \qquad (29)$$

As T and ${\Psi_s}^2$ are always positives, using the synergetic control makes the control constantly stable.

4 THE SENSORLESS MPPT ALGORITHM

To properly evaluate the MPPT technique, it is compared to a reference algorithm.

To choose the speed provided by the MPPT algorithm, it is very useful to use TSR MPPT as a reference method because it offers an excellent performance based on a correct measurement of the wind speed.

The TSR principle is very simple. It uses optimal tip ratio speed λ_{opt} provided by the manufacturer or simulations and the wind speed measured by an anemometer to have the reference speed which enable exploitation an optimal power from the wind where:

$$\Omega_{ref} = \frac{\lambda_{opt} Gv}{R} \qquad (30)$$

Where Ω_{ref} is the reference speed delivered to the synergetic control algorithm.

Due to the major drawback of this technique which is the presence of the mechanic sensor and difficulty of having a properly measured wind-speed value, a various sensorless MPPT algorithms have been developed.

Some of the sensorless algorithm are based on the knowledge of some system characteristics which can be very hard to define especially with large scale WECS.

4.1 The proposed fuzzy algorithm based-on HCS MPPT

The HCS algorithm is based on the measurement of the speed and active power. A step is added to the previous speed to become a new reference speed and the variation of ΔP is observed and that whey it is named perturb and observe algorithm (P&O). If $\Delta P > 0$, it means the step must be added to the speed until the power variation becomes negative when the step sign must be changing (figure 4).

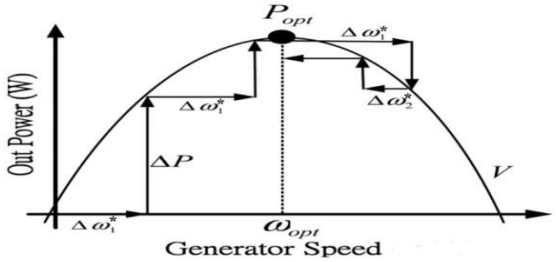

Figure 4. HCS principle.

The HCS algorithm follows the search-remember-reuse technique [19]. Its huge problem is choosing of step value in the HCS fixed-step. Using a small step, it takes much time to reach the maximum power point (MPP). In the opposite case there are serious oscillations in the active and reactive power, and both cases are denied. When using it in WECS none of the cases should be applied [20]. The HCS algorithm works properly without knowing anything about the system. This makes its integration with any WECS very easy.

There are many ways to overcome this drawback. One of them is using the fuzzy system based-on HCS. This enables an adaptive variable step. The step is big when the MPP is far away and smaller the closer we get to MPP.

There are three steps in the fuzzy system [20]:

- Fuzzification of the inputs transforming the numerical value to a linguistic character: N for negative, P for positive, S for small, M for middle, B for big and EZ for equal to zero;
- Table of rules (see Fig. 5);
- Defuzzification of the output to get a proper variable numerical value of the step.

dα \ dε	NB	NM	NS	EZ	PS	PM	PB
NB	EZ	EZ	EZ	NB	NB	NB	NB
NM	EZ	EZ	EZ	NM	NM	NM	NM
NS	NS	EZ	EZ	NS	NS	NS	NS
EZ	NM	NS	EZ	EZ	EZ	PS	PM
PS	PM	PS	PS	PS	EZ	EZ	EZ
PM	PM	PM	PM	EZ	EZ	EZ	EZ
PB	PB	PB	PB	EZ	EZ	EZ	EZ

Figure 5. Rules of the proposed fuzzy HCS.

5 ESTIMATION OF THE BDFIM SPEED BY AN EXTENDED KALMAN FILTER

Following the above, in the control process of BDFIM and MPPT algorithm, the machine speed needs to be measured to work correctly. In the past, the speed was measured only with a mechanic sensor coupled to the machine. Nowadays, for economic reasons and technical considerations, such as the reliability and the limited space in the wind turbine tower, researchers and manufacturers tend to estimate the speed without using a sensor.

There are different speed estimators. One such is the MRAS but its performances is inadequate to assure high efficiency and high precision, especially in WECS. The speed estimators performance has been improved by using an extended Kalman filter which provides an acceptable performance even in the presence of some noise.

The Kalman filter has been formerly used to estimate the state variables vector of linear systems. Then it was importantly extended by NASA to be used also for nonlinear systems [21], [22]. In a dynamic model of electric machines, adding a variable state, which is the speed to the state vector, transforms it to a nonlinear system where the speed becomes a variable and also a parameter [23].

The EKF algorithm loop follows below steps [24], [25] (see Fig. 6):

- Choosing the state model and its discretization;
- Initialisation of state variable vector $\hat{X}_k$ and prediction of the next estimated state variable and output vectors $\hat{X}_{k+1}$, $\hat{Y}_{k+1}$ from the EKF model;
- Setting the matrix of noise Q, R and covariance prediction matrix P;
- Calculation of Kalman gain K and its multiplication by error Y_e between measured vector Y_{mes} and output estimated EKF vector $\hat{Y}_{k+1}$ (Y_{est}) to have EKF estimation error vector EKF_e;
- Adding the EKF_e vector to state variable vector $\hat{X}_{k+1}$ in the EKF model updating P and returning to step 2.

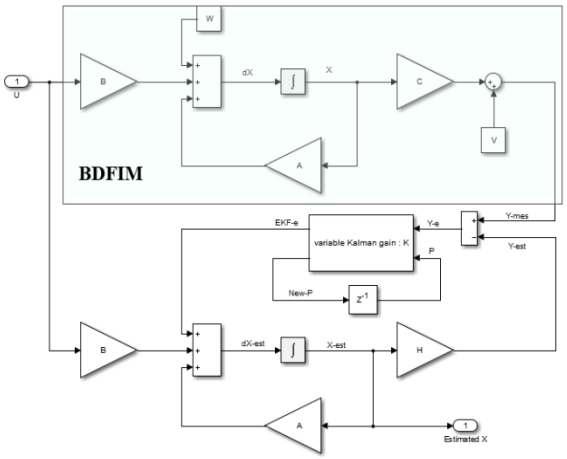

Figure 6. EKF structure.

5.1 EKF for the BDFIM

These have been developed many estimators for this machine. The most famous is MRAS based on the PW flux in [26]. Now we will build an EKF estimator and compare it to the MRAS estimator.

a- Choosing the BDFIM state model

At this stage, the fluxes and the machine speed are used as state variables vector and the PW dq-axes flux as measured vector despite not being directly measurable, but easily estimated by estimator (5.2 Section).

From equations (2), (3) and (4) BDFIM can like any system be described by the following state equations:

$$\begin{cases} \dot{X} = AX + BU + W \\ Y = CX + V \end{cases} \quad (31)$$

W is the system noise to make the model nearer to the reality and V is the measured noise present in the accuracy of the measurement tools of the flux estimator. Both noises are modelled by the Gaussian noise with the zero-mean value.

X is the state variable vector= $[\Psi_{dp} \quad \Psi_{qp} \quad \Psi_{dr} \quad \Psi_{qr} \quad \Psi_{dc} \quad \Psi_{qc} \quad \Omega]^T$, U is the control vector= $[V_{dp} \quad V_{qp} \quad 0 \quad 0 \quad V_{dc} \quad V_{qc} \quad Cr]^T$, B is the input matrix= $diag\left(\begin{bmatrix}1 & 1 & 1 & 1 & 1 & 1 & \frac{-1}{J}\end{bmatrix}\right)$, C is the output matrix= $\begin{bmatrix}1 & 0 & 0 & 0 & 0 & 0 & 0\\ 0 & 1 & 0 & 0 & 0 & 0 & 0\end{bmatrix}$ and A is the state matrix =

$$\begin{bmatrix} \frac{-R_p\sigma_c}{A_p} & w_p & \frac{R_pM_p}{A_pL_r} & 0 & -\frac{R_pA_1}{A_p} & 0 & 0 \\ -w_p & -\frac{R_p\sigma_c}{A_p} & 0 & \frac{R_pM_p}{A_pL_r} & 0 & -\frac{R_pA_1}{A_p} & 0 \\ \frac{R_rM_p}{A_rL_p} & 0 & -\frac{R_r}{A_r} & w_r & \frac{R_rM_c}{A_rL_c} & 0 & 0 \\ 0 & \frac{R_rM_p}{A_rL_p} & -w_r & -\frac{R_r}{A_r} & 0 & \frac{R_rM_c}{A_rL_c} & 0 \\ \frac{-R_cA_2}{A_c} & 0 & \frac{R_cM_c}{A_cL_r} & 0 & -\frac{R_c\sigma_p}{A_c} & w_c & 0 \\ 0 & -\frac{R_cA_2}{A_c} & 0 & \frac{R_cM_c}{A_cL_r} & -w_c & -\frac{R_c\sigma_p}{A_c} & 0 \\ \frac{-PA_3X_6}{J} & \frac{PA_3X_5}{J} & 0 & 0 & 0 & 0 & -\frac{f}{J} \end{bmatrix}$$

Where $\sigma_p = 1 - \frac{{M_c}^2}{L_cL_r}$, $A_p = L_p - \frac{{M_c}^2L_p}{L_cL_r} - \frac{{M_p}^2}{L_r}$, $A_r = L_r - \frac{{M_c}^2}{L_c} - \frac{{M_p}^2}{L_p}$, $A_c = L_c - \frac{{M_p}^2L_c}{L_pL_r} - \frac{{M_c}^2}{L_r}$, $w_r = w_p - P_1\Omega$ $A_1 = \frac{M_cM_p}{L_cL_r}$, $A_2 = \frac{M_cM_p}{L_pL_r}$, $A_3 = \frac{M_cM_p}{L_cL_rL_p - {M_p}^2L_c - {M_c}^2L_p}$, $P = P_1 + P_2$, $X_6 = \Psi_{qc}$ and $X_5 = \Psi_{dc}$.

b- *Discretization of the EKF model*

To get a good precision, the discrete-time EKF is used. The state equations of the EKF model in discrete time is:

$$\begin{cases} \hat{X}_{k+1} = A_d\hat{X}_k + B_dU \\ \hat{Y}_{k+1} = C_d\hat{X}_k \end{cases} \quad (32)$$

where $A_d = I + T_sA$, $B_d = T_sB$, $C_d = C$, I is the identity matrix and T_s is the discretization time.

c- *Set the noise matrices Q, R and the covariance prediction matrix P*

$Q = diag(10^{-6} * [1 \quad 1 \quad 1 \quad 1 \quad 1 \quad 1 \quad 1])$, $R = diag(10^{-3} * [1 \quad 1])$, and

$$P_{k+1} = J_d * P_k * (J_d)^T + Q \quad (33)$$

Where J_d is the Jacobian matrix of the discrete system which is the same as A_d save for the last colon which is: $\left[0 \quad 0 \quad -P_1T_s\hat{\Psi}_{qr} \quad P_1T_s\hat{\Psi}_{dr} \quad -PT_s\hat{\Psi}_{qc} \quad PT_s\hat{\Psi}_{dc} \quad 1 - \frac{T_sf}{J}\right]^T$.

d- *Calculus of Kalman gain K the estimation error EKFe*

The Kalman gain is the key of the EKF performance permitting the estimator to converge effectively. The gain is given by:

$$K_{k+1} = P_{k+1} * (H)^T * [H * P_{k+1} * (H)^T + R]^{-1} \quad (34)$$

and

$$EKF_e = K_{k+1}(Y_{mes} - \hat{Y}_{k+1}) \quad (35)$$

where H=C_d.

e- *Update P_{k+1} and $\hat{X}_k$*

P_{k+1} and $\hat{X}_k$ are updated as:

$$\begin{cases} (P_{k+1})_{new} = (I - K_{k+1} * H)P_{k+1} \\ (\hat{X}_k)_{new} = \hat{X}_k + EKF_e \end{cases} \quad (36)$$

5.2 Estimation of PW flux

The PW dq-axes flux is defined by a sensor which is difficult in most of the cases or by an estimator. It is used in the feedback of the SC controllers and to measure the vector for the EKF speed estimator.

There are different structures of the flux estimator like the ones based on the voltage model with or without DC-component correction, dynamic state estimator or the steady state estimator.

For our case, the steady state flux estimator is an optimal choice because it gives a good result specially after the start-up phase, and for the fixed PW supply frequency which makes the estimation process easier in a unified frame.

The equations for these estimators are:

$$\begin{cases} \Psi_{dp} = \frac{V_{qp} - R_p I_{qp}}{w_p} \\ \Psi_{qp} = \frac{R_p I_{dp} - V_{dp}}{w_p} \end{cases} \quad (37)$$

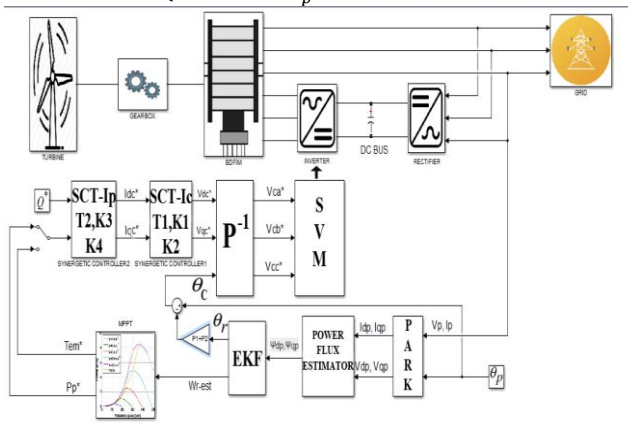

Figure 7. Scheme of each system.

6 SIMULATION RESULTS AND DISCUSSION

All the rest of the simulations are done in **MATLAB/SIMULINK** (2015a/8.5) environment. The main goal is to integrate the controlled BDFIM by a synergetic control in WECS with two MPPT algorithms. The first is the TSR MPPT which is used as a reference method. The second is the sensorless fuzzy-based HCS MPPT. To have the integration simulation is made in several steps.

First, the PW flux estimator is tested and used with the EKF to estimate the machine speed to evaluate the estimators performance.

The machine then controlled with the synergetic control. The CW and the PW current, active and reactive power, torque and the machine speed are controlled by the synergetic controllers.

A comparison with the conventional vector control with a PI controller is made to prove the outperformance of the synergetic control.

The next to follow are the control robustness tests against the parameter variation of the machine when the PW resistor and inductor values change during the simulation.

Finally, the system is integrated in the wind-energy conversion system with the TSR and fuzzy HCS MPPT algorithm to compare them and to prove the efficiency of the sensorless algorithm and removing the drawback in TSR MPPT.

The simulation parameters are shown in Figure 23.

6.1 BDFIM With EKF and PW flux estimator

As mentioned above, the EKF is used to estimate the BDFIM speed and the PW flux estimator provides the measured vector for EKF.

In the simulation the machine starts in its no-load state with CW short-circuited and at a 7.5 s instant, the CW is fed by a 4 Hz voltage system and then by a 8 Hz at a 8.5 s instant.

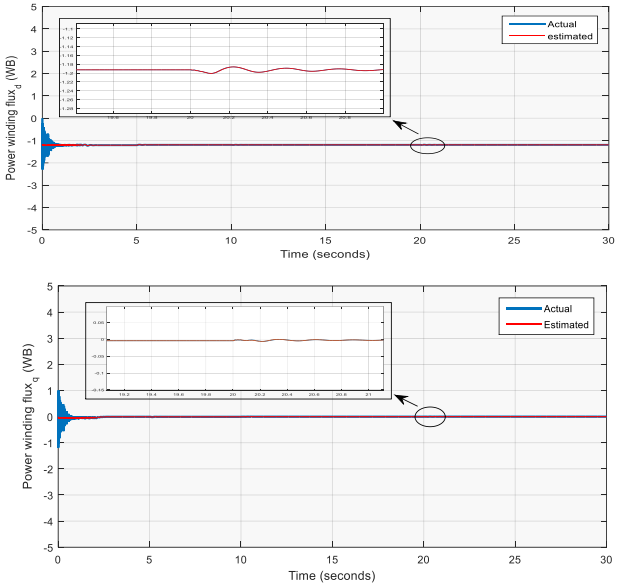

Figure 8. dq PW estimated flux.

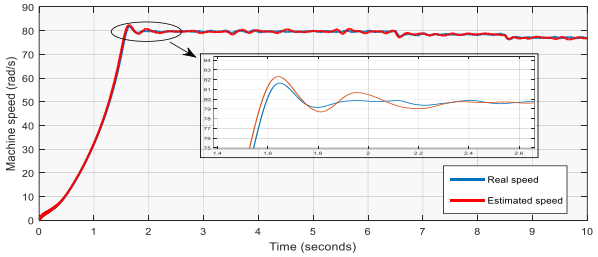

Figure 9. Real machine speed with the EKF-estimated speed.

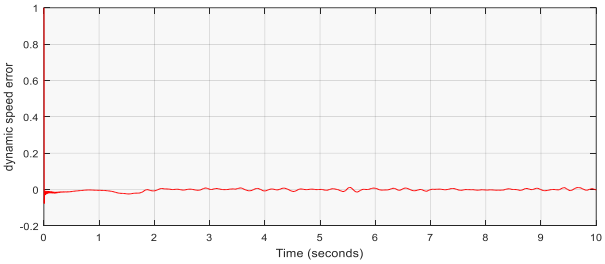

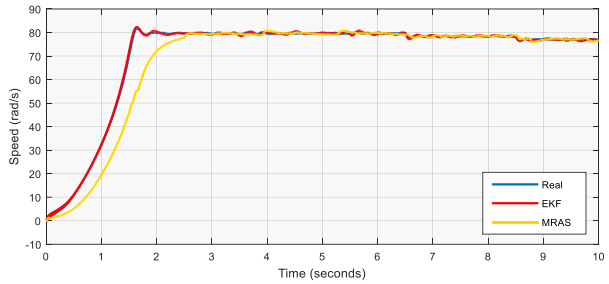

Figure 10 Dynamic speed error. The speed estimation of BDFIM by EKF compared to the MRAS estimator.

Figure 8 shows a good performance of the flux estimator. It effectively follows the real flux of the machine especially after start-up period, thus assuring a good EKF flux value.

Figure 9 shows that the speed estimated by EKF follows perfectly the machine real speed. It performs well even when machine varies its speed by the CW voltage frequency and in the presence of a serious model noise. The EKF compensates for the model and measurement noise and keeps on the actual speed with the reference speed. It is the best estimated one to work with it in the control process.

The dynamic speed error (see Fig. 10-a), is very small. Being less than 3%, it can be neglected and it proves the good efficiency of the proposed filter.

A comparison study between EKF and the MRAS (PW flux) suggested in [26] estimator prove the EKF superiority in estimating of the machine speed especially in the transitional regime where it is fast and its precision is improved (see Fig. 10-b).

The high EKF performance in its start-up period and transitional regime is very useful in the wind-energy conversion applications at occasions with a variable wind speed.

6.2 Synergetic control of BDFIM CW and PW current, power, torque and speed

The controllers given in Section 3.1 are now tested.

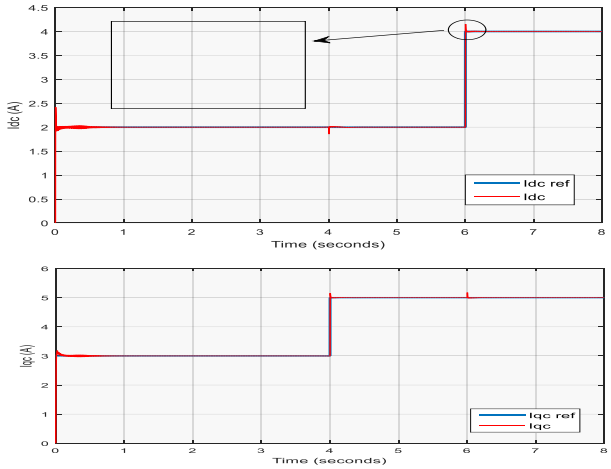

Figure 11. dq CW currents.

The CW current almost perfectly follows its reference. It is very fast with a minimum oscillations and overshoot (less than 3.75 %) when the references values change.

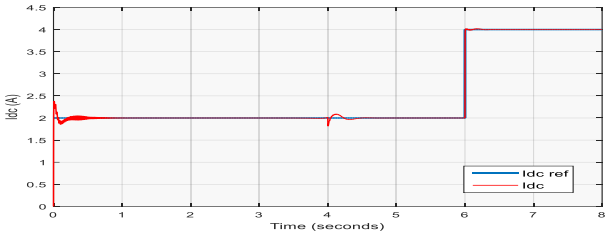

Figure 12. dq CW currents with K2=3.

When changing K_2, these is no overshoot but there are some troubles when the control becomes slower at a longer settling time and at high oscillations. For the integration of the control in WECS at a variable wind speed, this is a serious drawback.

The next to be assured a good performance is now the Ip controller.

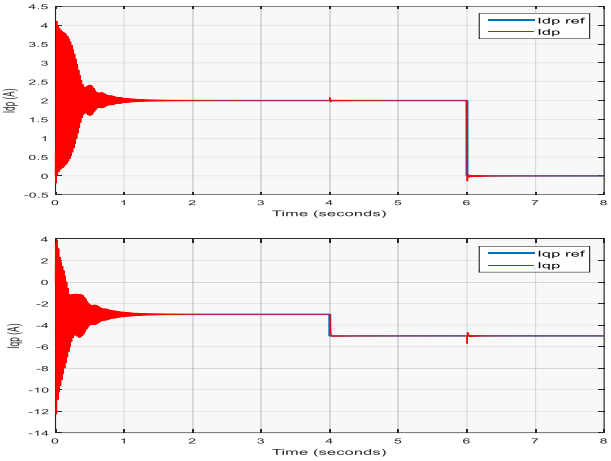

Figure 13. dq PW currents.

Similarly, as the CW current, the PW current keeps up perfectly its high performance, without serious oscillations, very small settling time and very limited overshoot.

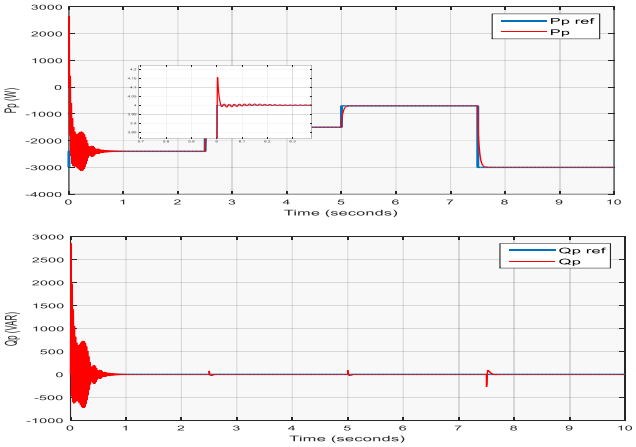

Figure 14. Active and reactive power.

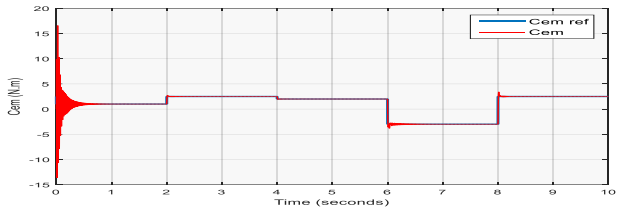

Figure 15. Machine torque.

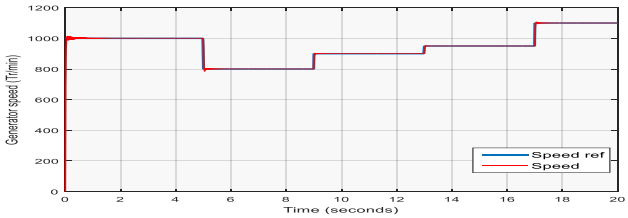

Figure 16. Machine speed.

As seen from the above figures, the controlled terms follow their references effectively, the performance is supreme, the control is very fast and there are no serious oscillations, overshoot and noise. Now that the evaluation of proposed control in a standard state is done, it is time to compare it with the conventional control methods and test its robustness before integrating it in WECS.

6.3 comparison with the conventional vector control

The I_c controller is compared to a PI controller to have an idea about the differences between the synergetic control and the vector control.

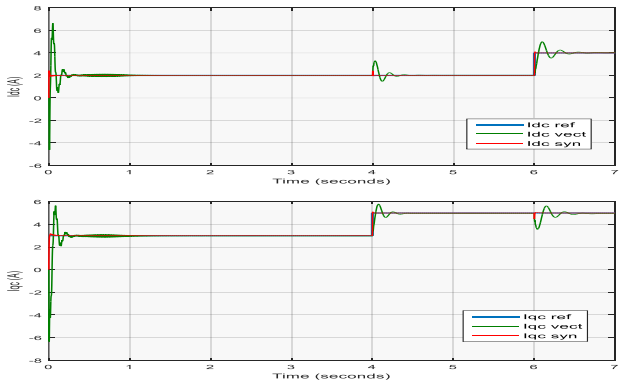

Figure 17. Comparison between the Ic synergetic controller with the PI controller (Kp=1.74 and Ki=996).

The synergetic control is better than the vector control with the PI controllers in all respects. It is faster, perturbations and overshoot are lower even when changing of the reference of the other channel. This altogether makes our synergetic control superior compared to the conventional vector control.

6.4 Robustness test of the proposed control

Robustness of the proposed control scheme against the parameter variation at an occurrence of a short circuit is evaluated. Robustness is a major parameter in the evaluation of any control method.

After 6 s, the value of PW resistance is decreased by 42.26 % (from 1.732 to 1 Ohm) and the PW inductance by 11.76 % (from 0.714 to 0.63 Henry).

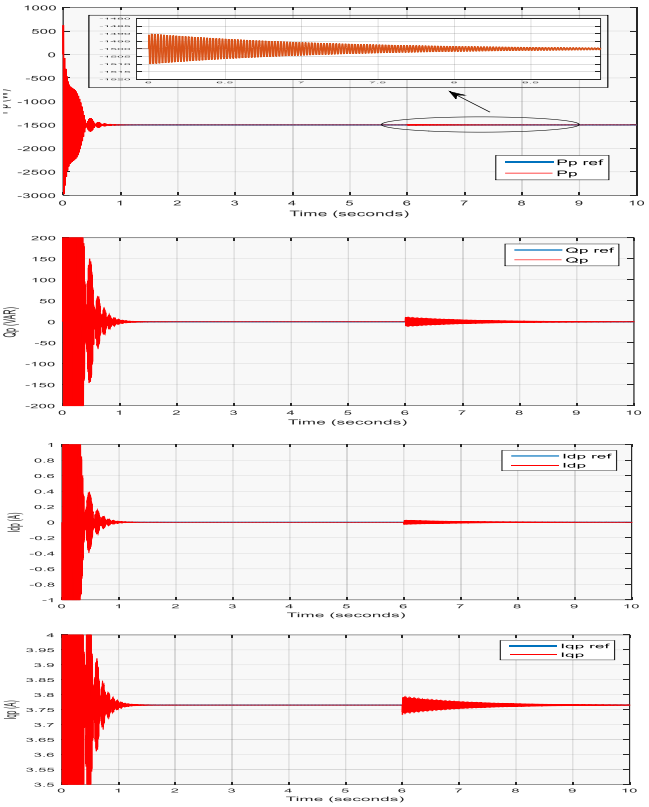

Figure 18. Parameter variation impact on the active and reactive power and PW currents.

As seen from the above figures, at the variation moment of the PW parameters, all the controlled parameters undergo perturbations in a form of small oscillations around the reference values. After some time, they decrease and almost disappear. It takes less than 4 s for the oscillations to become stable and neglectable and for the control channel to return the system to the desired point.

6.5 Integration of the system in the wind energy conversion system with the TSR and fuzzy HCS MPPT algorithm

The system is now integrated in WECS to evaluate under the impact of a variable wind speed while using two MPPT algorithms: TSR and fuzzy HCS.

a- <u>TSR MPPT algorithm:</u>

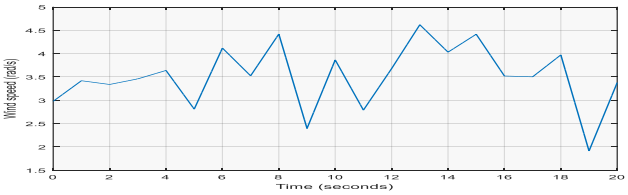

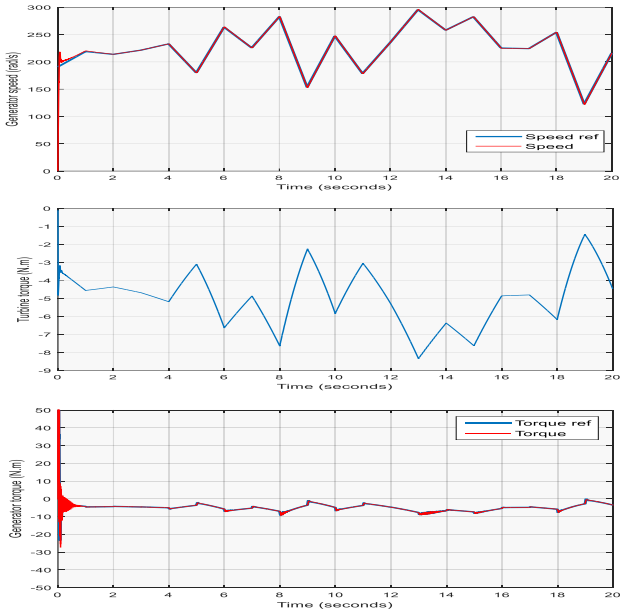

Figure 19. Wind speed, generator/reference speed, turbine torque and generator/reference torque.

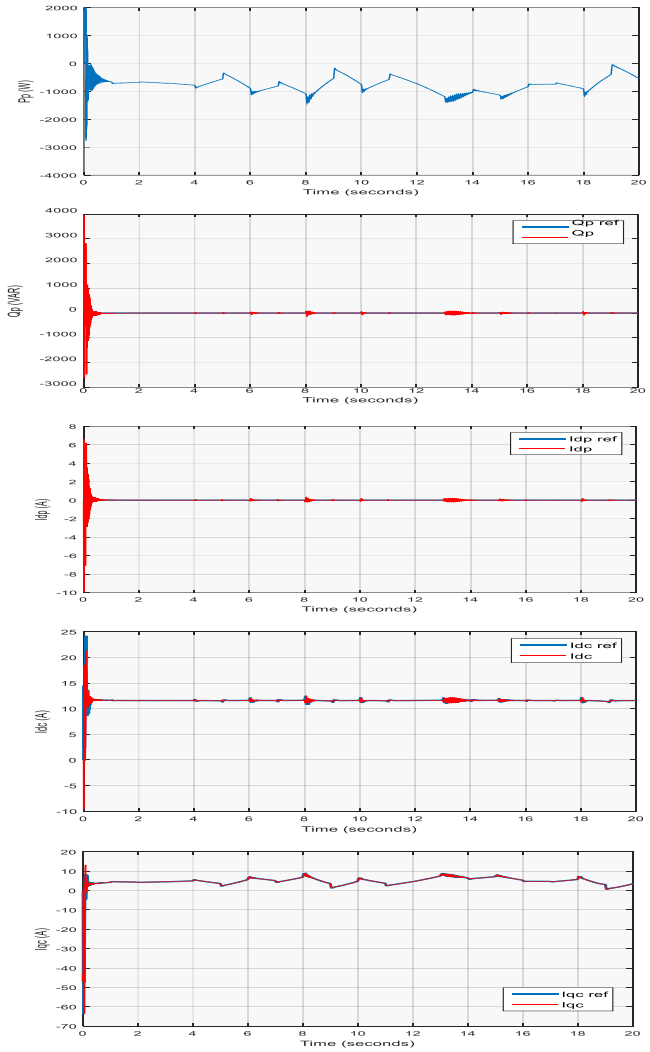

Figure 20. PW active and reactive power, Idp and the dq CW currents.

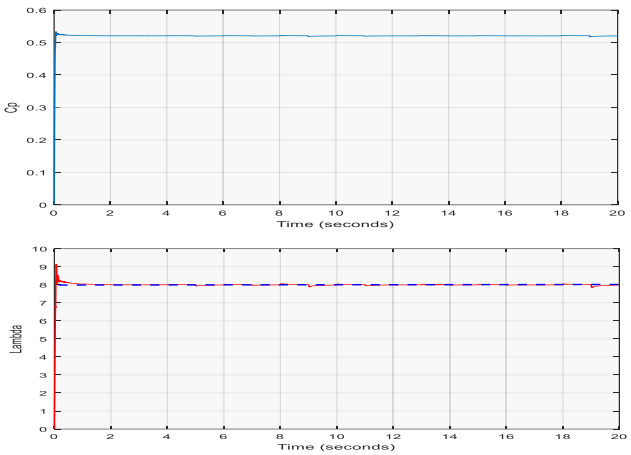

Figure 21. TSR power coefficient Cp and Lambda.

b- <u>Fuzzy based on HCS variable step MPPT</u>

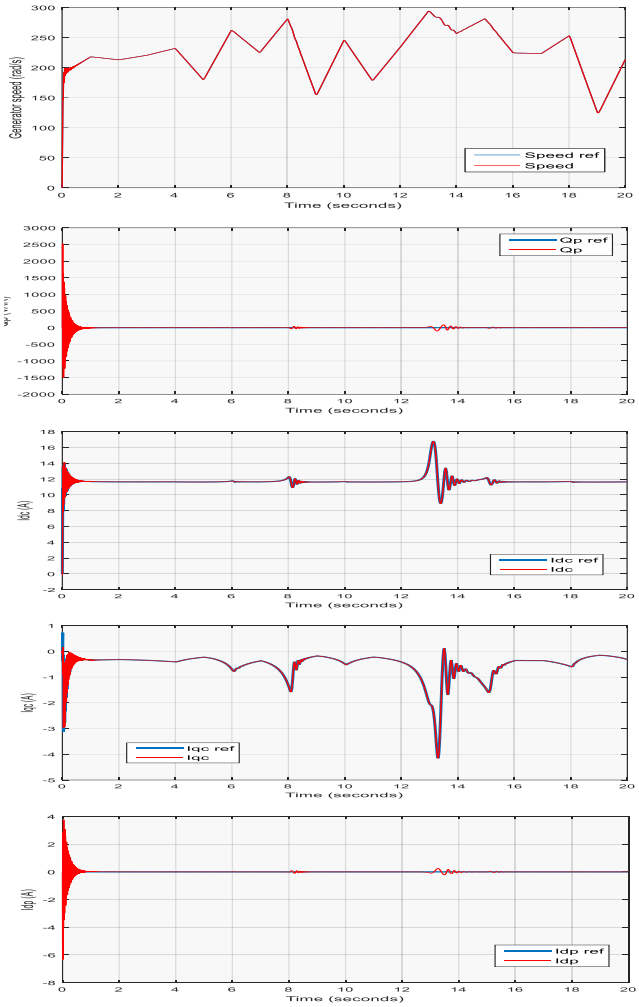

Figure 22. Speed, reactive power, dq CW current and Idp.

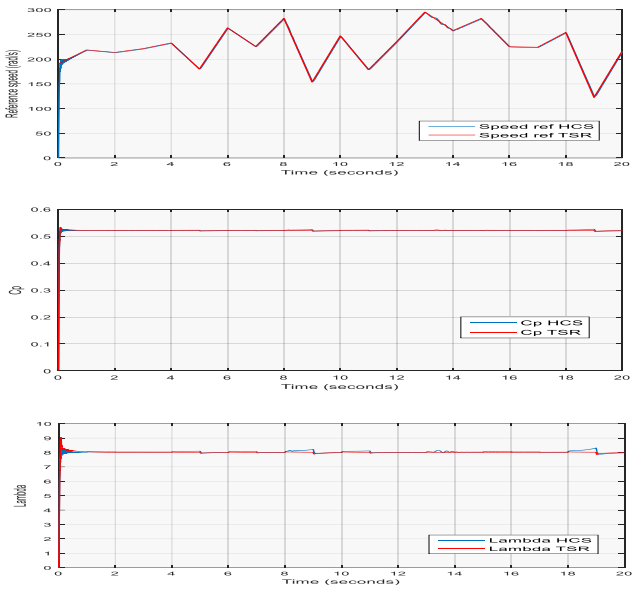

Figure 23. Comparison between TSR and fuzzy HCS algorithm (reference speed, Cp and Lambda).

As in the section 6.2, the synergetic control assures a reliable evaluation of the MPPT algorithm for the case of a solid ground.

In first made for TSR assures an excellent performance when it is supported by a proper wind speed which is very hard to achieve in reality but possible in simulation.

The reference speed keeps up with the wind speed variation fast and with a high precision which makes a very stable C_p and Lambda proves that the MPPT algorithm is very efficient and powerful.

The controlled currents, power, torque and speed follow exactly their references with neglectable oscillations and with outstanding performance.

Active power P_p is negative meaning that the machine works in the generator mode.

C_p is very stable and ≈ 53 % which is almost perfect and Lambda ≈ 8 which qualifies the TSR as a reference MPPT algorithm.

Fuzzy-based HCS MPPT provides a similar performance where all the variables follow their references very fast and without any noise or delay time. In figure 23-a, a comparison is made between TSR and fuzzy HCS MPPT algorithm in terms of their reference speed, Cp and Lambda show that the two algorithms provide a similar performance, with a little superiority of TSR especially in Lambda where there are small oscillations around the optimal value in the fuzzy-based HCS which is quite normal.

There are some differences between the two methods in their start-up phase when HCS works with a clean memory unlike TSR but it takes just less than 0.5 s to provides the same references.

Our simulation shows that fuzzy-based HCS with a variable step is a very powerful and reliable algorithm enabling a good performance similar to that of TSR without using any mechanical sensor (the major inconvenient of TSR) which avoids an incorrectly measured wind speed by the anemometer.

In the HCS MPPT algorithm, there is no need to know any data about the WECS characteristics, thus making it a standard method as such it can be used on any WECS of any dimensions and with any electric machine.

Type of parameters	designation	symbol	value
Turbine	Blade radius, Gain de gearbox, Air density, inertia, Cut-out wind speed	R, G, ρ, J_T, v_{max}	5m, 3, 1.225Kg/m^3, 21N.m.s/rad, 16m/s
BDFIM	PW, CW, and rotor resistors	R_p, R_c, R_r	1.732, 1.079, 0.474 (Ω)
	PW, CW, and rotor inductors	L_p, L_c, L_r	0.714, 0.1217, 0.1326 (H)
	Mutual inductors	M_p, M_c	0.2421, 0.0598 (H)

Figure 24. Simulation parameters.

7 CONCLUSION AND FUTURE WORK

This paper presents a novel robust sensorless synergetic control to be used for BDFIM integrated in WECS driven by TSR and fuzzy-based HCS MPPT.

The synergetic control of the first allows a robust, fast control high-performance and ensures an asymptotic stability of the closed-loop system in any operational state.

To increase the robustness of the proposed scheme, an extended Kalman filter (EKF) is used. The filter enables the mechanic sensor to keep the right estimated speed after estimating the PW flux.

After testing EKF, flux estimator, SC and its robustness they are integrated in WECS with fuzzy-based MPPT which ensures the maximum generated power without using any mechanic sensor or data about the WECS characteristics.

The simulation results prove the benefits of SC and EKF shows advantages of using sensorless powerful fuzzy HCS MPPT enabling the wind turbine system to operate at its optimal power at high wind speed and even in the presence of very a variable wind speed without using an anemometer or mechanic sensor. The scheme robustness is tested at variable parameter state and can as such contribute to wind energy system services, (voltage and frequency control ...).

In the future, our work is to develop the present scheme while it supported by intelligent Flywheel Energy Storage System.

REFERENCES

[1]. Sahin A. Progress and recent trends in wind energy. Energy Combustion. 2004;30(5):501–543.
[2]. Blaabjerg F, Ma K. Application of power electronics. wind energy system, Proceedings of the IEEE. 2017;105:2116-2131.
[3]. Kolesnikov A. Introduction of synergetic control. American Control Conference, June, Portland, Oregon, USA:3013–3016.
[4]. Kolesnikov A, Veselov G. A Synergetic Approach to the Modeling of Power Electronic Systems. Proc. Of COMPEL, Blacksburg, VA.
[5]. Awadallah A. Parameter Estimation of Induction Machines from Nameplate Data Using Particle Swarm Optimization and Genetic Algorithm Techniques. Electric Power Components and Systems. 2008:801-814. DOI: 10.1080/15325000801911393
[6]. Pao LY, Johnson KE. A tutorial on the dynamics and the control of wind turbines and wind farms. Am Control Conf. 2009.

[7]. Roberts PC. A Study of Brushless Doubly-Fed (Induction) Machines. University of Cambridge thesis. 2005:1.
[8]. Hopfensperger B, Atkinson D J, Lakin RA. Stator flux oriented control of a cascaded doubly-fed induction machine. Proc. Inst. Elect. Eng.—Elect. Power Appl. 1999;146(6):597–605.
[9]. Zhou D, Spee R, Alexander GC. Experimental evaluation of a rotor flux oriented control algorithm for brushless doubly-fed machines. IEEE Trans. Power Electron. 1997;12(1):72–78.
[10]. Löhdefink P, Dietz A, Möckel A. The brushless doubly fed induction machine as generator for small hydro power - machine design and experimental verification. Twelfth International Conference on Ecological Vehicles and Renewable Energies (EVER) conference. Monte Carlo, Monaco. 2017:11-13. DOI: 10.1109/EVER.2017.7935892
[11]. Tohidi S, Zolghadri MR, Oraee H, Oraee A. Dynamic Modeling of a Wind Turbine with Brushless Doubly Fed Induction Generator. 3rd Power Electronics and Drive Systems Technology conference (PEDSTC). 2012:490-494.
[12]. Williamson S, Ferreira AC, Wallace AK. Generalized theory of the brushless doubly-fed machine. Part 1: analysis. IEEE Proc.-Electr. Power Appl. 1997;144(2):111-122.
[13]. Williamson S, Ferreira AC. Generalized theory of the brushless doubly fed machine. Part 2: model verification and performance. IEE Proc.-Electr. Power Appl. 1997;144(2):123-129.
[14]. Poza FJ. Modélisation, Conception et Commande d'une Machine Asynchrone sans Balais Doublement Alimentée pour la Génération à Vitesse Variable. Institut National Polytechnique De Grenoble. 2009:125.
[15]. Kolesnikov A, Veselov G. Modern Applied Control Theory: Synergetic Approach. Control Theory. TRTU, Moscow. 2000.
[16]. Ni J, Liu C, Liu K, Pang X. Variable speed synergetic control for chaotic oscillation. power system nonlinear Dyn. 2014;78:681–690.
[17]. Laribi M, Ait Cheikh MS, Larbes C, Essounbouli N, Hamzaoui A. A sliding mode and synergetic control approach applied to induction motor. IEEE Proceedings of the 3rd International Conference on Systems and Control. October 2013.
[18]. Poza J, Oyarbide E, Sarasola I, Rodriguez M. Vector control design and experimental evaluation for the brushless doubly fed machine. IET Electric Power Applications. 2009;3(4):247-256.
[19]. Jogendra, S., Thongam, M.O, 2011, MPPT Control Methods in Wind Energy Conversion Systems. In Fundamental and Advanced Topics in Wind Power, ISBN: 978-953-307-508-2. URL: http://www.intechopen.com/books/fundamental-and-advancedtopics-in-wind-power/mppt-control-methods-in-wind-energy-conversion-systems
[20]. Beghdadi M, Kouzi, Ameur A. New design of an optimized synergetic control by hybrid BFO-PSO for PMSG integrated in wind energy conversion system using variable step HCS fuzzy MPPT. Springer Smart Energy Empowerment in Smart and Resilient Cities (ICAIRES 2019). 2020;102:30-40. Doi.org/10.1007/978-3-030-37207-1_4
[21]. McElhoe BA. An Assessment of the Navigation and Course Corrections for a Manned Flyby of Mars or Venus. IEEE Transactions on Aerospace and Electronic Systems. 1966:613–623. DOI: 10.1109/TAES.1966.4501892
[22]. Smith GL, Schmidt SF, McGee LA. Application of statistical filter theory to the optimal estimation of position and velocity on board a circumlunar vehicle. National Aeronautics and Space Administration. 1962.
[23]. Kim YR, Sul SK, Park MH. Speed Sensorless Vector Control of Induction Motor Using Extended Kalman Filter. IEEE Transactions on Industry Applications. 1994;30(5):1225-1233.
[24]. Gunabalan R, Subbiah V, Rami Reddy B. Sensorless Control of Induction Motor with Extended Kalman Filter on TMS320F2812 Processor. in International Journal of Recent Trends in Engineering. 2009;2(5):14-19.
[25]. Serhoud H, Benattous D. Sensorless optimal power control of brushless doubly-fed machine in wind power generator based on extended Kalman filter. Int J Syst Assur Eng Manag. 2013:57–66. DOI: 10.1007/s13198-012-0141-6
[26]. Zhu Y, Zhang X and Liu S, Study on speed sensorless vector control of Brushless Doubly-Fed Machine, International Conference on Consumer Electronics, Communications and Networks (CECNet). 2011:780-783. DOI: 10.1109/CECNET.2011.5768887

Mohammed Beghdadi obtained his Bachelor's and Master's degrees in Electrical Engineering, electrical Machinery Division, from El-Bayed University in 2016 and 2018. He is currently a PhD student in Electrical Control at the University of Laghouat.

Katia Kouzi obtained her engineering and Magister degrees in electrical engineering in 1998 and 2002. She received the doctorate degree in electrical control from the University of Batna in 2008. Her research interests are focused on advanced sensorless control through artificial intelligence techniques, renewable energy. She is currently a professor in electrical engineering in University of Laghouat.